FULL PAPER

Aggregation-Induced Emission

**ADVANCED
FUNCTIONAL
MATERIALS**

www.afm-journal.de

Malonitrile-Functionalized Tetraphenylpyrazine: Aggregation-Induced Emission, Ratiometric Detection of Hydrogen Sulfide, and Mechanochromism

Ming Chen, Rui Chen, Yang Shi, Jianguo Wang, Yanhua Cheng, Ying Li, Xuedong Gao, Yun Yan, Jing Zhi Sun, Anjun Qin, Ryan T. K. Kwok, Jacky W. Y. Lam, and Ben Zhong Tang*

Development of new aggregation-induced emission (AIE) luminogens has been a hot research topic because they thoroughly solve the notorious aggregation-caused quenching effect confronted in conventional fluorogens and their promising applications in, for example, organic light-emitting diodes, chemo- and biosensors and bioimaging. Many AIE luminogens (AIEgens) have been prepared but most of them are silole, tetraphenylethene, distyrylanthracene, and their derivatives. In this work, based on the skeleton of tetraphenylpyrazine (TPP), a new AIEgen, named TPP-PDCV, is generated by functionalizing TPP with malonitrile group. TPP-PDCV can serve as a sensitive ratiometric fluorescent probe for detecting hydrogen sulfide with high speciality and low detection limit of down to 0.5×10^{-6} M. The mechanism for such detection is fully investigated and deciphered. Unlike most reported mechanochromic AIEgens, which undergo turn-off or -on emission or emission bathochromic shift in the presence of external stimuli, TPP-PDCV exhibits an abnormal and reversible mechanochromism with hypsochromic effect. These indicate that TPP-PDCV possesses a huge potential for high-tech applications through rational modification of TPP core.

1. Introduction

Luminescent materials are crucial for human beings to illuminate and deliver information in organic light-emitting diodes based white-light lamps and full-color displays.[1] They also act as visual tools for substrate analysis and tracking of life process.[2] However, for real-word applications, they are often utilized as solid films or nanoparticles where their molecules are aggregated. Unfortunately, conventional luminogens with planar structures often show weaker emission or even become nonemissive upon aggregation due to the aggregation-caused quenching (ACQ) effect, which greatly hampers their practical use.[3] In 2001, Tang and co-workers observed an abnormal photophysical phenomenon, termed "aggregation-induced emission (AIE)," in a series of propeller-like

Dr. M. Chen, Dr. J. Wang, Dr. Y. Cheng, Dr. Y. Li, Dr. R. T. K. Kwok,
Dr. J. W. Y. Lam, Prof. B. Z. Tang
Department of Chemistry
Hong Kong Branch of Chinese National Engineering Research
Center for Tissue Restoration and Reconstruction
Institute for Advanced Study
Division of Biomedical Engineering, Division of Life Science
State Key Laboratory of Molecular Neuroscience and Institute
of Molecular Functional Materials
The Hong Kong University of Science and Technology
Clear Water Bay, Kowloon, Hong Kong, China
E-mail: tangbenz@ust.hk

Dr. M. Chen, Dr. J. Wang, Dr. Y. Cheng, Dr. Y. Li, Dr. R. T. K. Kwok,
Dr. J. W. Y. Lam, Prof. B. Z. Tang
Guangdong Provincial Key Laboratory of Brain Science
Disease and Drug Development
HKUST Shenzhen Research Institute
Shenzhen 518057, China

R. Chen, Y. Shi, Prof. J. Z. Sun
MOE Key Laboratory of Macromolecular Synthesis and Functionalization
Department of Polymer Science and Engineering
Zhejiang University
Hangzhou 310027, China

X. Gao, Prof. Y. Yan
Beijing National Laboratory for Molecular Sciences
State Key Laboratory for Structural Chemistry of Unstable and Stable
Species
College of Chemistry and Molecular Engineering
Peking University
Beijing 100871, China

Prof. A. Qin, Prof. B. Z. Tang
Guangdong Innovative Research Team
State Key Laboratory of Luminescent Materials and Devices
South China University of Technology
Guangzhou 510640, China

luminogens, in which aggregation plays a positive instead of negative role in enhancing luminescence.[4] The emergence of AIE luminogens (AIEgens) thoroughly overcomes the difficulties confronted in ACQ molecules. Under the guidance of the restriction of intramolecular motion as the mechanism for the AIE phenomenon, many AIEgens based on silole, tetraphenylethene, distyrylanthracene, and triphenylethene have been tailored.[5] These AIEgens have been found to possess efficient light emission in the solid state and wide high-tech applications, but they show different drawbacks. For example, siloles are difficult to synthesize and purify. Besides, they are unstable in basic medium. On the other hand, AIEgens carrying double bonds undergo photoisomerization, photo-oxidation, and photoactivation in the presence of UV irradiation, which complicates our understanding on their AIE phenomenon and also affects their materials performance.[6] Thus, it is desirable to develop new AIE systems without the above shortcomings.[7]

Recently, we found that tetraphenylpyrazine (TPP) is AIE-active and displays many advantages, such as easy preparation, facile modification, good stability, and tunable emission.[8] However, the type of TPP-based AIEgens presented so far is limited and their study mainly focuses on their electroluminescence and nonlinear optics.[9] Through intelligent design of molecular structure, more functionalities, such as fluorescence sensing and stimuli-responsive emission change should be able to derive from TPP-based AIEgens.

Hydrogen sulfide (H_2S) was considered as a poisonous, corrosive, and flammable natural gas with unpleasant smell. The toxicity of H_2S is comparable to that of carbon monoxide. It can bind with iron in the mitochondrial cytochrome enzymes, prohibiting cellular respiration, and resulting in apnea asphyxiate.[10] Excessive exposure to H_2S can also influence the nervous system to cause headache, dizziness, irritability, and mental confusion. The permissible exposure limit of H_2S for human is 10 ppm for 8 h time-weighted average. On the other hand, H_2S is also an important endogenous gas transmitter with high concentration (10×10^{-6} to 600×10^{-6} M) in the brain of bovine, rat, and human.[11] H_2S is also found to be associated with various physiological processes, such as vasodilation, cell growth, antioxidation, and regulation of inflammation. The abnormal level of H_2S is related to symptoms such as Alzheimer's disease and diabetes.[12] Since fluorescence-based techniques are more selective, sensitive, and noninvasive for substrate analysis, a few H_2S probes with turn-on or ratiometric responses have been designed based on the mechanisms of nucleophlic reaction, azide reduction, and quencher removal.[13] However, most of them show response time of longer than 20 min, and their detection is thus time consuming.[14] Additionally, accurate quantitative analysis of H_2S concentration is often difficult. Recently, our group developed a turn-on AIE probe for detecting H_2S with tunable detection threshold in two handling steps.[15] Thus, it is particularly attractive to design AIEgen-based ratiometric fluorescent probe to detect H_2S with advantages of quick response, accurate quantitative analysis, simple operation process and low background noise.

Mechanochromic luminescent materials have found potential applications in security inks, logical gates, optical displays, and information storage for their capability to alter their lig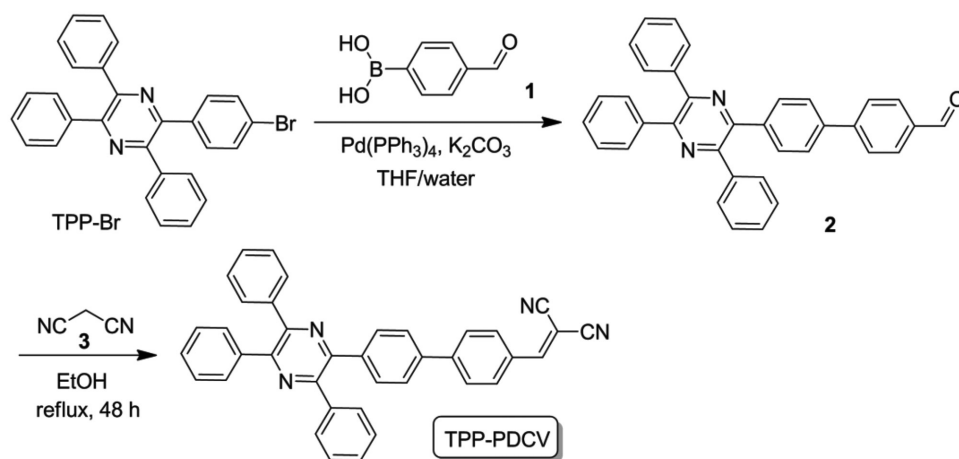ht emissions by external force.[16] The emergence of AIEgens significantly promotes the development of this field because almost all the mechanochromic luminescent materials are employed in the aggregate state.[17] The high emission efficiency of AIEgens upon aggregation enables remarkable switching of luminescence signals to achieve a high contrast ratio. Besides, the twisted and flexible conformation of AIEgens makes them to pack loosely in aggregate state, making them to change their molecular conformation and hence the light emission with ease under external force. Most of the mechanochromic luminescent AIEgens reported so far show bathochromic shift in their light emission in response to external force because the energy of the frontier molecular orbital is altered and the energy gap becomes narrow upon molecular conformational change.[18] Our group also developed some mechanochromic luminescent systems with emission turn-off and turn-on response. For example, AIEgens with crystallization-induced emission enhancement characteristics often show strong fluorescence in the pristine powder (crystal state), whereas their emissions are almost lost in the amorphous state by grinding.[19] In contrast, AIE-active diaminomaleonitrile-functionalized Schiff bases display an opposite behavior. In the crystalline state, they emit no light due to the severe π–π stacking. When such interaction is broken by external stimuli, intense emission was observed.[20] Park and co-workers also employed the photoinduced electron transfer or fluorescence resonance energy transfer strategy to design AIEgen-based mechanochromic luminescent systems with emission turn-on or multicolor response.[21] Nevertheless, nearly no paper on mechanochromic luminescent AIEgens with hypsochromic effect has been reported, though such materials are indispensable members in the mechanoluminescent family and provide more opportunities for designing smart materials.

With this idea in mind, in this work, we developed a new TPP-based AIEgen, namely TPP-PDCV, with polar malonitrile functionality. Because malonitrile group is a strong electron-withdrawing group and TPP is relatively electron-donating, TPP-PDCV thus possesses a donor (D)–acceptor (A) structure and shows green or orange emission in the aggregate state, which is much redder than our previously reported derivatives. The malonitrile functionality also enables TPP-PDCV to function as a ratiometric fluorescent probe to detect H_2S with fast response, high sensitivity, and good selectivity. Due to the different molecular packing in the aggregate state, TPP-PDCV forms crystalline powders emitting different colors. It exhibits a rare reversible mechanochromic effect with emission blue-shift aided by grinding and annealing. It indicates that the TPP-based AIEgen is a multifunctional material with versatile potential applications. Thus, the results presented here are expected to generate research enthusiasm for creating functional AIEgens based on the TPP skeleton.

2. Results and Discussion

2.1. Synthesis and Characterization of TPP-PDCV

TPP-PDCV was prepared by Suzuki coupling reaction of TPP-Br[9a] and 4-formylphenylboronic acid (1) followed by a condensation reaction of the resulting intermediate (2) with malonitrile (3) (**Scheme 1**). The crude product was purified by

**ADVANCED
SCIENCE NEWS**
www.advancedsciencenews.com

**ADVANCED
FUNCTIONAL
MATERIALS**
www.afm-journal.de

Scheme 1. Synthetic route to TPP-PDCV.

column chromatography and the desirable product was isolated in a satisfactory yield. Its structure was characterized using ^{1}H and ^{13}C NMR and high-resolution mass spectroscopies with satisfactory data corresponding to its structure (Figures S1–S5, Supporting Information). Thermogravimetric analysis (TGA) shows that TPP-PDCV exhibits a 5% weight loss at 316 °C, suggesting that it possesses a good thermal stability (Figure S6, Supporting Information).

2.2. Optical Properties

After structural characterization, we studied the photophysical property of TPP-PDCV. The UV spectrum of TPP-PDCV exhibits two absorption peaks at 308 and 372 nm with molar absorptivities of 2.02×10^4 and 4.04×10^4 L mol^{-1} cm^{-1}, respectively (**Figure 1**). The absorption at the shorter wavelength was ascribed to the π–π^* transition of the TPP chromophore, while the longer-wavelength absorption was attributed to charge transfer from the electron-donating TPP core to the peripheral electron-accepting malonitrile group.

Since TPP is AIE-active, will TPP-PDCV also exhibit the AIE characteristic? To answer this question, we checked the photoluminescence (PL) of TPP-PDCV in dimethyl sulfoxide (DMSO)/water mixtures containing various water fractions (f_W). TPP-PDCV emits a weak orange PL at 580 nm in DMSO. Gradual increasing the f_W from 10% to 40% in the DMSO/water mixtures weakens the emission accordingly (**Figure 2**). At $f_W = 50\%$, an emission peak was emerged at 511 nm, whose intensity was less enhanced upon further increment in f_W. The maximum PL enhancement is ≈12-fold. The active intramolecular motion of TPP-PDCV molecules in DMSO has consumed the energy of the exciton through nonradiative relaxation channel, thus rendering the dye molecules weakly emissive. Because TPP-PDCV possesses a D–A structure, the increase in polarity of the DMSO/water mixture with increasing f_W will strengthen the twisted intramolecular charge-transfer (TICT) effect to cause emission quenching.[22] Molecular aggregation may take place at $f_W \geq 50\%$, which activates the RIR process to cause emission enhancement. On the other hand, the TPP-PDCV molecules in the interior of the aggregates are less

affected by the surrounding solvent environment. This diminishes the TICT effect and cause a blue-shift in the emission.[23] Shuai and co-workers carried out a detailed study on the bluer emission in the aggregate state than in the solution state and proposed that this is due to the smaller reorganization energy in the former than in the later.[24]

2.3. H$_2$S Sensing

The presence of malonitrile functionality in TPP-PDCV may enable it to act as fluorescent probe to detect nucleophilic species. Among various analytes, H$_2$S detection is of particular interest in consideration of its significance in affecting the environmental safety, tuning life process, and controlling some human diseases. The excessive exposure of H$_2$S can have an
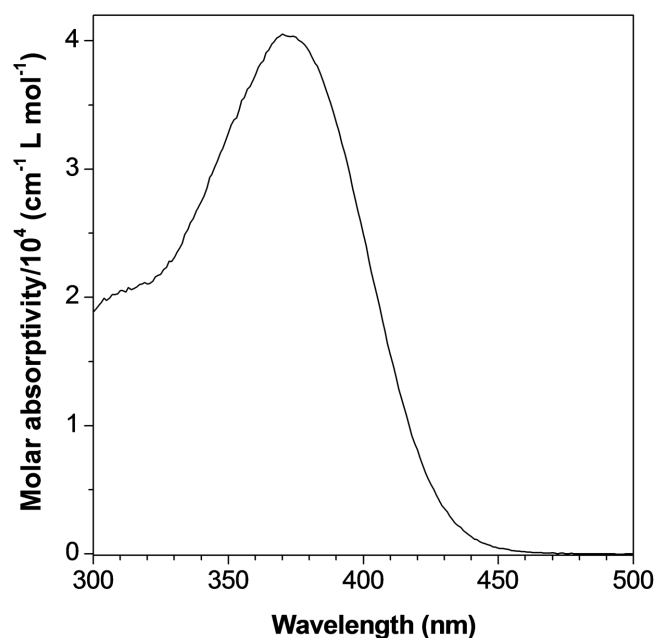

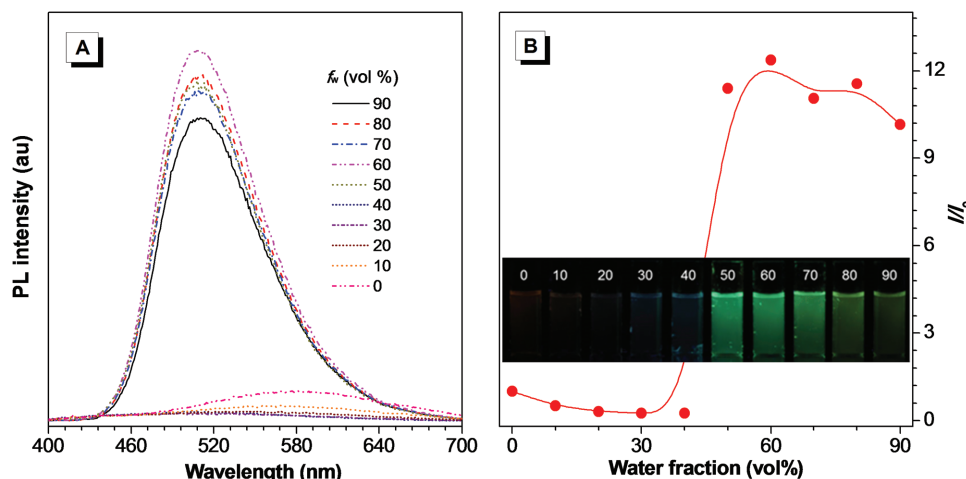**Figure 1.** UV–vis spectrum of TPP-PDCV in DMSO, [TPP-PDCV] = 10×10^{-6} M.

**ADVANCED
SCIENCE NEWS**
www.advancedsciencenews.com

**ADVANCED
FUNCTIONAL
MATERIALS**
www.afm-journal.de

Figure 2. A) PL spectra of TPP-PDCV in DMSO/water mixtures with different water fractions (f_W) [TPP-PDCV] = 10×10^{-6} M, λ_{ex} = 372 nm. B) Plot of relative PL intensity (I/I_0) versus the composition of DMSO/water mixture of TPP-PDCV, where I_0 = PL intensity in pure DMSO solution. Inset: photographs of TPP-PDCV in DMSO/water mixtures with different water fractions taken under irradiation of 365 nm UV light.

obvious impact on the human health in a short time. The catabolism of H_2S is found to be fast in the body. However, most of the reported H_2S probes show slow response time of more than 20 min.[14] We thus carried out the time-dependent PL measurement to study the kinetic of the present probe. As shown in **Figure 3**A, the probe exhibits an orange-yellow emission at 565 nm in DMSO/phosphate buffered saline (PBS) mixture (25×10^{-6} M, v/v = 9:1) in the absence of NaHS. After addition of 10 equivalent NaHS, H_2S was generated and the orange–yellow emission was quenched gradually with time. At the same time, a blue emission peak with enhanced intensity appears at 429 nm. Clearly, the AIE probe is ratiometric with remarkable color variation. The ratio between the emission intensity at 429 and 565 nm continues to increase in 10 min. Afterwards, the value remains almost constant, demonstrating that the detection can be finished in a short time (Figure 3B).

Fluorescent titration of the probe with NaHS with concentration range from 0×10^{-6} to 500×10^{-6} M shows that the probe can respond to H_2S at concentration of below 250×10^{-6} M. The plots of relative PL intensity (I_{429}/I_{565}) versus NaHS concentration at $0–75 \times 10^{-6}$ and $150–225 \times 10^{-6}$ M demonstrate good linear relationship, which means that the probe is suitable for quantitative H_2S detection (Figure 3C,D). In addition, the detection limit was deduced to be as low as 0.5×10^{-6} M (S/N = 3). This indicates that the probe is highly sensitive to H_2S, making it to find wide biological applications and promising use in environmental safety estimation (Figure S7, Supporting Information).

To evaluate the specificity of the probe, we first checked its PL response to various anions. As shown in **Figure 4**, except CO_3^{2-}, all the anions exert little effect on the relative PL intensity. TPP-PDCV also shows weak response to biospecies, such as cysteine (Cys), homocysteine (Hcy), and glutathione (Glu). Recently, Wang and co-workers reported a malonitrile-incorporated metal–organic framework for H_2S detection.[25] However, it simultaneously shows remarkable response to Cys. Clearly, the present probe possesses better selectivity. Our group previously developed malonitrile-decorated silole for differentiating

Cys and Hcy from Glu.[26] We also found that a malonitrile-modified TPE could selectively detect GSH rather than Cys and Hcy.[27] Coupled with the present results, all these indicate that the AIE luminogenic core plays a crucial role in determining the sensing behavior.

We and other research groups proposed that the nucleophilic addition reaction of analyte to the malonitrile group of the probe served as the sensing mechanism.[28] Will it also hold true in the present case? To unveil the cause, we carried out a large-scale organic reaction of TPP-PDCV with NaHS under similar conditions for the H_2S detection and found that two spots with different polarities were observed in the TLC plate using hexane/dichloromethane mixture (v/v = 2: 1) as developing solvent. These spots emit deep blue light when excited by 365 nm UV irradiation. The first spot with low polarity shows a negligible absorption under 254 nm UV light, suggesting that it is a minor product generating in trace amount. In contrast, the second spot possesses a higher polarity and produces as a major product. After purification of the main product by silica-gel column chromatography, a disulfide compound named TPP-2PS was collected, whose structure was confirmed by NMR spectroscopy. Its high-resolution mass spectrum shows m/z value of 1011.3552, which was correlated with the theoretical value (1011.3555) and was assigned to [TPP-2PS + H]+ (**Figure 5**C; Figure S8, Supporting Information). Such result is surprising and differs from those reported previously. Disulfide compounds are usually obtained through the oxidation reaction of thiol molecules.[29] Thus, it is believed that a thiol intermediate, namely TPP-PSH, was also generated, whose self-coupling formed TPP-2PS. To prove its existence, we synthesized TPP-PSH according to the synthetic route shown in Scheme S1 (Supporting Information). The obtained product was characterized by NMR and mass spectroscopies with satisfactory data (Figures S9–S17, Supporting Information). The synthesized TPP-PSH shows a same polarity as that of the first spot in the TLC plate, and oxidizes quickly even in the solid state to form polar TPP-2PS. Thus, the detection mechanism become clear: the probe first undergoes a nucleophilic addition reaction with
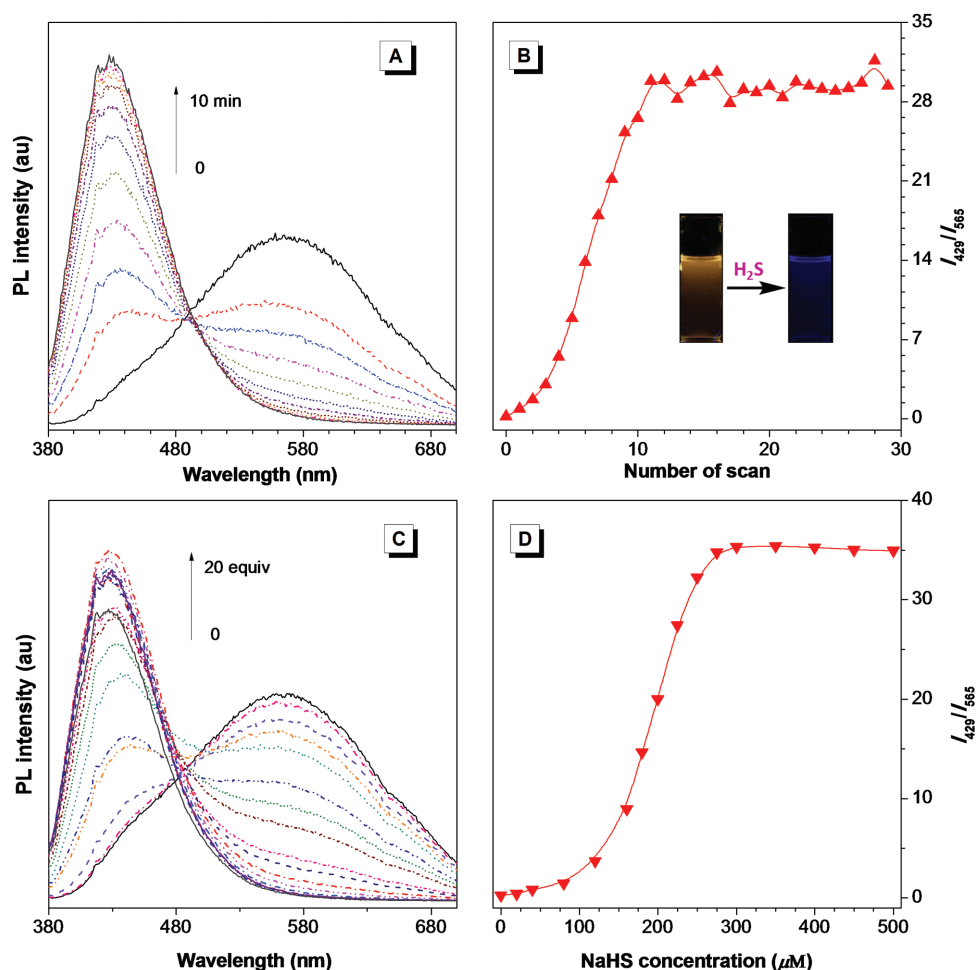
Figure 3. A) Change of PL spectrum of TPP-PDCV treated with NaHS in DMSO/PBS buffer mixture (v/v 9:1) with time, [TPP-PDCV] = 25×10^{-6} M, [NaHS] = 250×10^{-6} M, [PBS] = 10×10^{-3} M; pH = 7.40, λ_{ex} = 372 nm. B) Plot of relative PL intensity (I_{429}/I_{565}) versus the number of scan in a total time of 25 min, where I_{429} and I_{565} are the PL intensity at 429 and 565 nm. Inset: fluorescent photographs of TPP-PDCV before and after reaction with NaHS. C) PL spectra of TPP-PDCV titrated with different NaHS concentrations from 0×10^{-6} to 500×10^{-6} M in DMSO/PBS buffer mixture (v/v 9:1) for 10 min, [TPP-PDCV] = 25×10^{-6} M, [PBS] = 10×10^{-3} M; pH = 7.40, λ_{ex} = 372 nm. D) Plot of relative PL intensity (I_{429}/I_{565}) versus NaHS concentration.

H_2S followed by possible hemolysis and hydrolysis to form TPP-PSH as intermediate. Oxidation reaction then takes place quickly between TPP-PSH molecules to generate TPP-2PS as a final product.

Time-dependent UV–vis spectroscopic study reveals that the maximum absorption of TPP-PDCV at 372 nm disappears gradually with increasing its reaction time with H_2S. A new peak, on the other hand, arises at 350 nm (Figure S18, Supporting Information). It is somewhat expected because the D–A structure of the probe was destroyed after nucleophilic addition. This diminishes the intramolecular charge transfer effect to result in a blue-shift in the maximum absorption. Accordingly, the emission of the probe changes from orange–yellow to deep blue in the presence of NaHS, providing a good platform for the visual analysis of H_2S with high contrast. It is worth noting that the deep blue emission was derived from the aggregates of the generated TPP-2PS because it is AIE-active, as suggested by the same emission color of the purified TPP-2PS powder shown in Figure S19 (Supporting Information). In DMSO/PBS buffer mixture (v/v 9:1), TPP-PDCV is molecularly dissolved

because of its high polarity. However, after reaction with H_2S, the produced TPP-2PS shows a low polarity but a higher rigidity. Collectively, all these factors induce the formation of TPP-2PS aggregates in DMSO/PBS buffer mixture.

2.4. Unique Mechanochromism

Two kinds of powders of TPP-PDCV with green and orange-yellow emissions at 511 and 545 nm were obtained by recrystallization from acetone and toluene, respectively (**Figure 6**A). Interestingly, upon mechanical grinding, the emission of powder B shifts to lower wavelength and the color changes from orange-yellow to green at 522 nm. However, its original emission color was recovered after annealing its ground powder at 180 °C. The orange-yellow and green-emissive powders can be interconverted to each other many times without fatigue aided by grinding and annealing (Figure 6B,C). Besides, direct annealing of the pristine green-emissive powder at the same temperature can partially afford orange-yellow
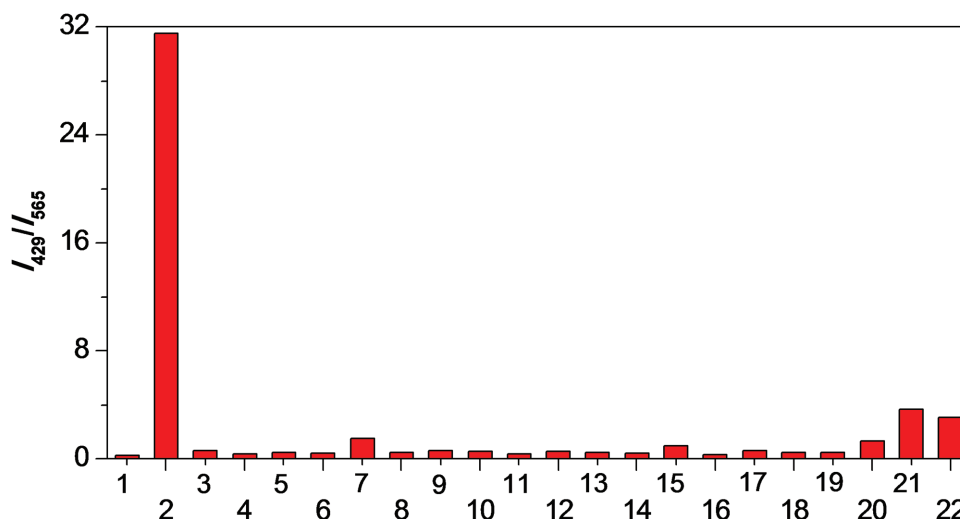
Figure 4. Change of relative PL intensity (I_{429}/I_{565}) of TPP-PDCV treated with different anions and thiols in DMSO/PBS buffer mixture (v/v = 9:1) for 10 min, where I_{429} and I_{565} are the PL intensity at 429 and 565 nm. [TPP-PDCV] = 25×10^{-6} M, [analyte] = 250×10^{-6} M, [PBS] = 10×10^{-3} M; pH = 7.40, λ_{ex} = 372 nm. (1: Blank; 2: H_2S; 3: AcO^-; 4: $B(C_6H_5)_4^-$; 5: Br^-; 6: ClO^-; 7: CO_3^{2-}; 8: F^-; 9: HCO_3^-; 10: IO_4^-; 11: N_3^-; 12: NO_2^-; 13: NO_3^-; 14: $P_2O_7^{4-}$; 15: OH^-; 16: $PH_2O_2^-$; 17: $S_2O_3^{2-}$; 18: SCN^-; 19: SO_4^{2-}; 20: Cys; 21: Hcy; 22: Glu. All counter ions are Na^+).

emissive powder resembled that of annealed ground powder B. Such mechanochromic behavior with hypsochromic shift effect is very unique in AIE systems because almost all the reported mechanochromic AIEgens show turn-on or -off emission and emission bathochromic shift in response to external stimuli. Thus, this provides more opportunities to develop new smart materials, as for example, security inks, logic gates, and information storage.
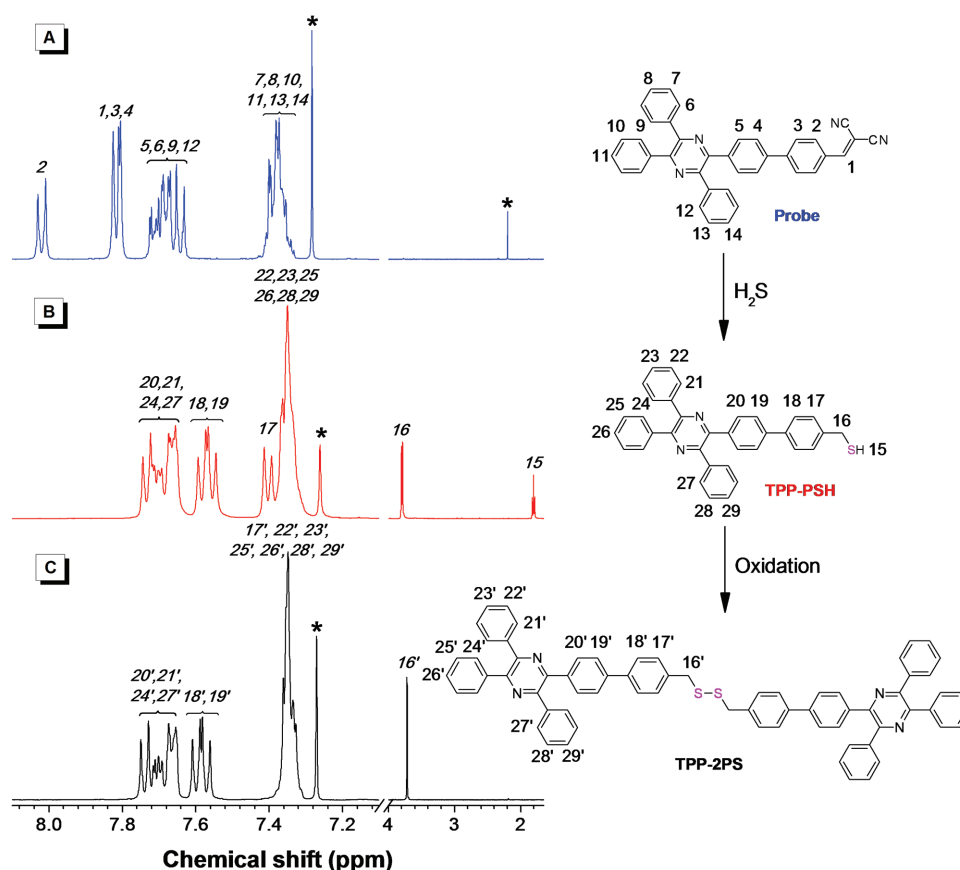

Figure 5. ¹H NMR spectra of A) TPP-PDCV, B) TPP-PSH and C) TPP-2PS in CDCl₃.
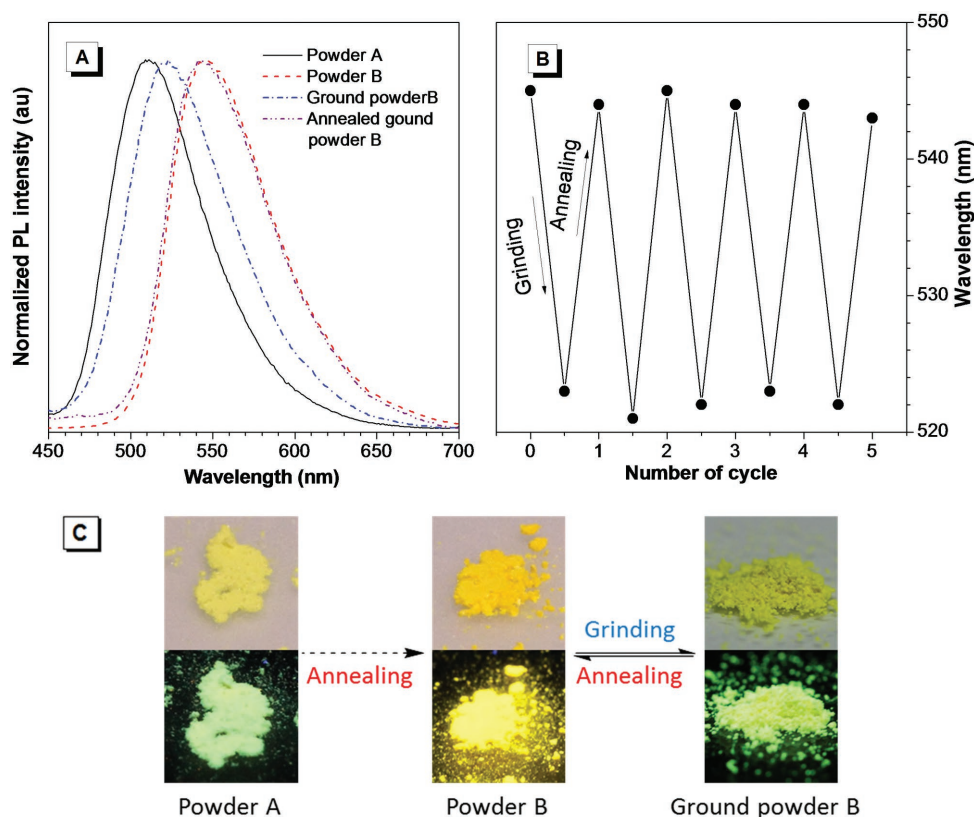
Figure 6. A) PL spectra of powder A, powder B, and ground powder B and annealed ground powder B. B) Switching of the emission wavelength between powder B and ground powder B by repeated grinding and annealing. C) Photographs of different powders taken under (upper) daylight and (lower) 365 nm UV light.

Why distinct emission behavior was observed in various powders of the same luminogen and what is the cause for the abnormal mechanochromic effect? To answer these questions, analysis of powder A and B by powder X-ray diffraction (PXRD) and differential scanning calorimetry (DSC) was carried out. The PXRD diffractograms of powder A and powder B show sharp diffraction peaks but are of different patterns, suggesting that they are all crystalline but with different molecular packing (**Figure 7**A,B). The diffraction peaks at 2θ of 4.2° and 5.7° of powder A and powder B correspond to d-spacings of 2.10 and 1.55 nm, respectively, according to the Bragg's law ($2d\sin\theta = n\lambda$). On the other hand, the length of TPP-PDCV calculated from its optimized molecular conformation by using DFT/B3LYP/6-31G (d) is 2.17 nm. Thus, the TPP-PDCV molecules are likely to pack in a head-to-head fashion in powder A, whereas a head-to-tail packing is preferred in powder B (Figure S20, Supporting Information). Such arrangements are similar to those of H-aggregates and J-aggregates.[30] The fluorescence quantum yield of powder A and powder B measured by an integrating sphere was 12.0% and 53.7%, respectively (**Table 1**). Thus, powder B shows redder emission in higher efficiency. Such phenomenon is well correlated with the emission behavior between H-aggregates and J-aggregates, which thereby further supports the conclusion drawn from the PXRD analysis.

The smaller d-spacing of powder B (1.55 nm) than powder A (2.10 nm) suggests that the molecules of the former pack in a
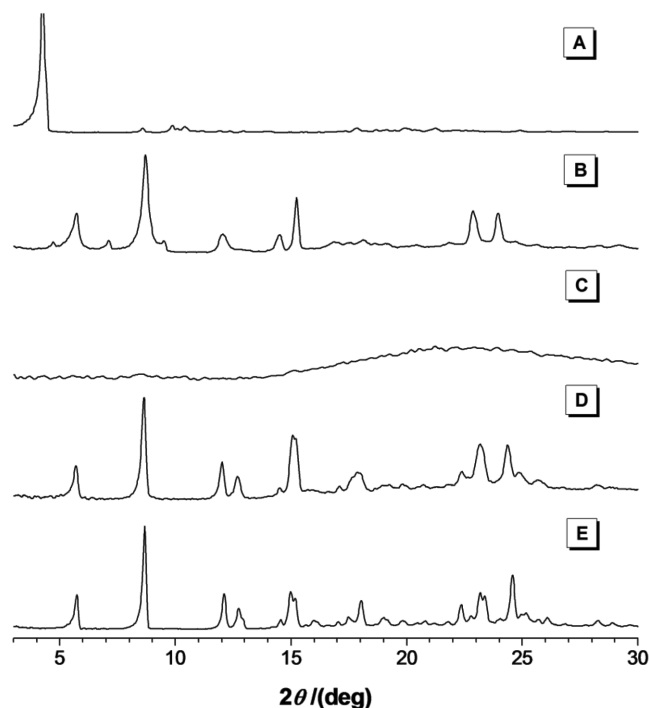

Figure 7. PXRD diffractograms of A) powder A, B) powder B, C) ground powder B, D) annealed ground powder B, and E) partial annealed powder A.

Table 1. Photophysical properties of different powders of TPP-PDCV.

	λ_{em} [nm][a]	Φ_F [%][b]	τ [ns][c]	k_r [10^8 S^{-1}][d]	k_{nr} [10^8 S^{-1}][e]
Powder A	511	12.0	0.91	1.3	9.6
Powder B	545	53.7	6.83	0.79	0.68

[a]λ_{em}, emission maximum; [b]Φ_F, fluorescence quantum yield measured by an integrating sphere; [c]τ, fluorescence lifetime; [d]k_r, rate of relative decay = Φ_F/τ; [e]k_{nr}, rate of nonradiative decay = $(1 - \Phi_F)/\tau$.

more dense fashion. This leads to stronger intermolecular interaction and hence a higher melting points (227 °C) than powder A (146 °C) as determined by DCS analysis (Figure S22A,B, Supporting Information). On the other hand, the loosely molecular packing of powder A introduces more free space for the molecules to rotate even in the aggregate state to dissipate the excitation energy nonradiatively. That may explain why powder A is less emissive than powder B. The excited-state decay of the powders are estimated according to the formulas of $k_r = \Phi_F/\tau$ and $k_{nr} = (1 - \Phi)/\tau$, where k_r and k_{nr} are the radiative and nonradiative decay rates, and Φ_F and τ are the absolute quantum yield and excited-state lifetime, respectively (Table 1; Figure S21, Supporting Information). The calculated k_r of powder A is 1.3×10^8 S^{-1} and is slightly higher than that of powder B (0.79×10^8 S^{-1}). However, its k_{nr} (9.6×10^8 S^{-1}) is more than 10-fold higher than powder B (0.68×10^8 S^{-1}). This suggests that the molecular motion in powder A is indeed apt to take place to decrease the luminescence efficiency.

After grinding powder B, an amorphous solid was formed because its PXRD diffractogram shows almost no diffraction peaks (Figure 7C). As the ordered *J*-aggregates are destroyed in the presence of external stimuli, the emission of powder B blue shifts. The original orange-yellow emission color was recovered by annealing the ground powder B, as suggested by the large similarity in the PXRD diffractogram of the annealed ground powder with the pristine one (Figure 7D). The DSC thermogram of the ground powder B exhibits peaks at 157 and 222 °C associated with the recrystallization and melting point of the powder, further confirming that the crystalline structure is easy to reform by the annealing process (Figure S22C, Supporting Information).

3. Conclusions

In this work, we prepared a new TPP-based AIEgen (TPP-PDCV) carrying malonitrile functional group. TPP-PDVC can function as a ratiometric fluorescent probe to detect H$_2$S. The probe shows good selectivity against competitive anions and biothiols with a low detection limit of 0.5×10^{-6} M. The detection mechanism is systematically investigated and involves first a nucleophilic addition reaction of analyte to the probe followed by oxidation reaction of the generated adduct. TPP-PDCV forms crystals with different emission colors attributed to the possible formation of *J*-aggregates and *H*-aggregates. The redder emissive powder exhibits a mechanochromic phenomenon with hypsochromic effect in the presence of external stimuli because of the reversible transformation between the crystalline and amorphous states. This work not only provides a novel AIEgen

responding to external chemical and force stimuli but also exhibits more opportunities for designing TPP-containing AIE materials with advanced functionalities.

4. Experimental Section

Materials and Instrumentation: All the commercially available chemicals including NaHS were purchased from Sigma Aldrich, Alfa Aesar, or J&K chemistry and used directly without further purification. TPP-Br was prepared according to our previously reported literature.[9a] Tetrahydrofuran (THF) was distilled from sodium benzopheone ketyl under dry nitrogen immediately before use. ^{1}H and ^{13}C spectra were measured on a Bruker AVIII 400 MHz NMR spectrometer using CDCl$_3$ as solvent. High-resolution mass spectra (HRMS) were recorded on a GCT premier CAB048 mass spectrometer operated in MALDI-TOF mode. UV–vis absorption spectra were recorded on a Cary 50 Conc spectrophotometer. PL spectra were recorded on a HORIBA spectrofluorometer. The absolute Φ_F values were measured using a Hamamatsu Quantaurus-QY C11347 spectrometer. The PL decay curves were measured on an Edinburgh FLSP920 fluorescence spectrophotometer equipped with a xenon laser arc lamp (Xe900), a microsecond flash lamp (uF900), and a picosecond pulsed diode laser (EPL-375), and a closed-cycle cryostat (CS202*I-DMX-1SS, Advanced Research Systems). TGA was carried out on a TA TGA Q5000 under nitrogen at a heating rate of 10 °C min^{-1}. DSC was carried out on a TA DSC Q1000 under nitrogen at a heating rate of 10 °C min^{-1}. PXRD patterns were recorded on D/Max-2550pc machine and Cu Kα radiation ($\lambda = 1.54059$Å) was used at 40 kV and 250 mA. The scan rate was 5° min^{-1}.

Synthesis of TPP-PCHO (2): TPP-PCHO was synthesized according to the synthetic route shown in Scheme 1. Briefly, into a 250 mL round bottom flask was added 3 g (6.5 mmol) of TPP-Br, 1.17 g (7.8 mmol) of 4-formylphenylboronic acid, 372 mg (0.32 mmol) of Pd(PPh$_3$)$_4$, 100 mL of THF, and 13.8 g of K$_2$CO$_3$ (dissolved in 50 mL of water) under nitrogen. The mixture was stirred under reflux overnight. Afterward, the mixture was cooled to room temperature, diluted with dichloromethane, and washed with aqueous NaCl solution. The collected organic phase was condensed under reduced pressure and the crude product was purified on a silica-gel column using hexane/dichloromethane (v/v = 1:1) as eluent. A white powder of 2.79 g (5.7 mmol) was obtained in a yield of 88.2%. ^{1}H NMR (400 MHz, CDCl$_3$), δ (ppm): 10.06 (s, 1H), 7.97–7.95 (d, 2H), 7.80–7.77 (d, 4H), 7.72–7.66 (m, 6H), 7.63–7.61 (d, 2H), 7.39–7.32 (m, 9H). ^{13}C NMR (100 MHz, CDCl$_3$), δ (ppm): 191.3, 148.0, 147.9, 146.9, 145.8, 139.1, 138.1, 137.8, 137.7, 134.7, 130.0, 129.7, 129.3, 128.2, 128.1, 127.8, 127.7, 127.0, 126.6.

Synthesis of TPP-PDCV: Into a 500 mL round bottom flask was added 2.76 g (5.7 mmol) of **2**, 0.76 g (11.5 mmol) of malonitrile, and 300 mL of dry ethanol under nitrogen. The mixture was stirred under reflux for 2 d. Afterwards, the mixture was cooled to room temperature and condensed under reduced pressure. The crude product was purified on a silica-gel column with hexane/dichloromethane (v/v = 2:1) as eluent to afford 1.58 g (2.94 mmol) of green powder in a yield of 52.1%. ^{1}H NMR (400 MHz, CDCl$_3$), δ (ppm): 8.00–7.98 (d, 2H), 7.80–7.77 (m, 5H), 7.70–7.60 (m, 8H), 7.38–7.31 (m, 9H). ^{13}C NMR (100 MHz, CDCl$_3$), δ (ppm): 159.1, 148.7, 148.6, 148.5, 147.3, 146.6, 139.3, 138.8, 138.3, 131.4, 130.7, 129.9, 128.9, 128.8, 128.4, 128.3, 128.0, 127.1, 112.8, 113.9, 82.1. HRMS (MALDI-TOF): *m/z* 536.2016 [M$^+$, calcd for 536.2001].

Synthesis of TPP-2PS: Into a 10 mL Schlenk tube was added 10 mg (0.019 mmol) of TPP-PDCV, 2 mL of DMSO, and 10.4 mg (0.19 mmol) of NaHS dissolved in 0.2 mL of water. The mixture was stirred at room temperature for 30 min. Afterward, the mixture was poured into water and extracted with dichloromethane three times. The collected organic phase was condensed under reduced pressure and the crude product was purified on a silica-gel column using hexane/dichloromethane (v/v = 2:1) as eluent to afford a white powder. ^{1}H NMR (400 MHz,

CDCl$_3$), δ (ppm): 7.74–7.64 (m, 8H), 7.60–7.55 (m, 4H), 7.35–7.31 (m, 11H). HRMS (MALDI-TOF): m/z 1011.3552 [(M+1)$^+$, calcd. for 1011.3555].

Synthesis of TPP-PMe (5): TPP-PMe was synthesized according to the synthetic route shown in Scheme S1 (Supporting Information). The procedure was similar to that of TPP-PCHO except that 4-formylphenylboronic acid was replaced by 4-methylbenzeneboronic acid, pinacol ester. A white powder of 0.92 g (1.94 mmol) was obtained in a yield of 89.8%. ^{1}H NMR (400 MHz, CDCl$_3$), δ (ppm): 7.73–7.64 (m, 9H), 7.56–7.51 (m, 4H), 7.36–7.32 (m, 10H), 2.39 (s, 3H). ^{13}C NMR (100 MHz, CDCl$_3$), δ (ppm): 147.8, 147.7, 147.4, 140.6, 138.0, 137.9, 137.0, 136.8, 136.4, 130.0, 129.3, 128.9, 128.1, 128.0, 127.7, 127.6, 126.3, 126.1, 20.6.

Synthesis of TPP-PBr (6): Into a 100 mL round bottom flask was added 500 mg (1.05 mmol) of 5, 2.6 mg (0.01 mmol) of benzoyl peroxide, and 50 mL of CCl$_4$. The mixture was allowed for stir at 80 °C overnight, while 197 mg (1.1 mmol) of N-bromobutanimide was added in several times during the reaction. Afterward, the mixture was condensed under reduced pressure and the crude product was purified on a silica-gel column using hexane/dichloromethane (v/v = 2:1) as eluent. A white powder of 400 mg (0.72 mmol) was obtained in a yield of 68.6%. ^{1}H NMR (400 MHz, CDCl$_3$), δ (ppm): 7.74–7.72 (d, 2H), 7.70–7.64 (m, 6H), 7.64–7.53 (m, 4H), 7.46–7.44 (d, 2H), 7.35–7.30 (m, 9H). ^{13}C NMR (100 MHz, CDCl$_3$), δ (ppm): 147.8, 147.2, 140.0, 139.7, 137.8, 137.1, 136.5, 129.8, 129.3, 129.0, 128.1, 127.7, 127.6, 126.8, 126.3, 32.7.

Synthesis of TPP-PTA (8): Into a 50 mL round bottom flask was added 300 mg (0.54 mmol) of 6, 65 mg (0.57 mmol) of potassium thiolacetate, 20 mL of methanol and 2 mL of THF. The mixture was stirred at room temperature overnight. Afterward, the mixture was condensed under reduced pressure and the crude product was purified on a silica-gel column using hexane/THF (v/v = 10:1) as eluent. A white powder of 160 mg (0.29 mmol) was obtained in a yield of 53.8%. ^{1}H NMR (400 MHz, CDCl$_3$), δ (ppm): 7.72–7.64 (m, 8H), 7.56–7.52 (m, 4H), 7.37–7.32 (m, 11H), 4.16 (s, 2H), 2.36 (s, 3H). ^{13}C NMR (100 MHz, CDCl$_3$), δ (ppm): 195.1, 148.4, 147.9, 140.7, 139.5, 138.5, 137.5, 137.0, 130.3, 129.9, 129.3, 128.7, 128.4, 128.3, 127.3, 126.8, 33.2, 30.4.

Synthesis of TPP-PSH: Into a 50 mL round bottom flask was added 20 mg (0.036 mmol) of 8, 10 mL of 0.02 M aqueous NaOH solution and 10 mL of methanol. The mixture was stirred at room temperature overnight. Afterward, dilute hydrochloric acid was added to quench the reaction and the mixture was extracted with dichloromethane three times. The organic phase was condensed under reduced pressure and the crude product was purified on a silica-gel column using hexane/dichloromethane (v/v = 4:1) as eluent. A white powder of 6 mg was obtained in a yield of 32.5%. ^{1}H NMR (400 MHz, CDCl$_3$), δ (ppm): 7.73–7.65 (m, 8H), 7.59–7.54 (m, 4H), 7.41–7.39 (d, 2H), 7.36–7.34 (9H), 3.80–3.78 (d, 2H), 1.82–1.78 (t, 1H). ^{13}C NMR (100 MHz, CDCl$_3$), δ (ppm): 148.4, 147.9, 140.8, 140.5, 139.3, 138.5, 137.4, 130.3, 129.9, 128.7, 128.5, 128.4, 128.3, 127.4, 126.8, 28.7. HRMS (MALDI-TOF): m/z 506.1828 [M$^+$, calcd. for 506.1817].

Supporting Information

Supporting Information is available from the Wiley Online Library or from the author.

Acknowledgements

Conflict of Interest

The authors declare no conflict of interest.

Keywords

[1] a) A. C. Grimsdale, K. L. Chan, R. E. Martin, P. G. Jokisz, A. B. Holmes, *Chem. Rev.* **2009**, *109*, 897; b) O. Ostroverkhova, *Chem. Rev.* **2016**, *116*, 13279; c) L. Ying, C. L. Ho, H. Wu, Y. Cao, W. Y. Wong, *Adv. Mater.* **2014**, *26*, 2459.

[2] a) Z. Gu, L. Yan, G. Tian, S. Li, Z. Chai, Y. Zhao, *Adv. Mater.* **2013**, *25*, 3758; b) G. Hong, S. Diao, A. L. Antaris, H. Dai, *Chem. Rev.* **2015**, *115*, 10816; c) M. Montalti, A. Cantelli, G. Battistelli, *Chem. Soc. Rev.* **2015**, *44*, 4853.

[3] J. B. Birks, *Photophysics of Aromatic Molecules*, Wiley, London **1970**.

[4] a) J. Luo, Z. Xie, J. W. Y. Lam, L. Cheng, H. Chen, C. Qiu, H. S. Kwok, X. Zhan, Y. Liu, D. Zhu, B. Z. Tang, *Chem. Commun.* **2001**, 1740; b) B. Z. Tang, X. Zhan, G. Yu, P. P. S. Lee, Y. Liu, D. Zhu, *J. Mater. Chem.* **2001**, *11*, 2974.

[5] a) J. Mei, N. L. C. Leung, R. T. K. Kwok, J. W. Y. Lam, B. Z. Tang, *Chem. Rev.* **2015**, *115*, 11718; b) J. Mei, Y. Hong, J. W. Y. Lam, A. Qin, Y. Tang, B. Z. Tang, *Adv. Mater.* **2014**, *26*, 5429; c) D. Ding, K. Li, B. Liu, B. Z. Tang, *Acc. Chem. Res.* **2013**, *46*, 2441; d) Q. Li, Z. Li, *Adv. Sci.* **2017**, *4*, 1600484.

[6] a) Z. Zhao, B. He, B. Z. Tang, *Chem. Sci.* **2015**, *6*, 5347; b) Z. Yang, W. Qin, N. L. C. Leung, M. Arseneault, J. W. Y. Lam, G. Liang, H. H. Y. Sung, I. D. Williams, B. Z. Tang, *J. Mater. Chem. C* **2016**, *4*, 99; c) Z. He, L. Shan, J. Mei, H. Wang, J. W. Y. Lam, H. H. Y. Sung, I. D. Williams, X. Gu, Q. Miao, B. Z. Tang, *Chem. Sci.* **2015**, *6*, 3538.

[7] a) Y. Duan, C. Ju, G. Yang, E. Fron, E. Coutino-Gonzalez, S. Semin, C. Fan, R. S. Balok, J. Cremers, P. Tinnemans, Y. Feng, Y. Li, J. Hofkens, A. E. Rowan, T. Rasing, J. Xu, *Adv. Funct. Mater.* **2016**, *26*, 8968; b) M. S. Yuan, X. Du, F. Xu, D. E. Wang, W. J. Wang, T. B. Li, Q. Tu, Y. Zhang, Z. Du, J. Wang, *Dyes Pigm.* **2015**, *123*, 355.

[8] a) M. Chen, L. Li, H. Nie, J. Tong, L. Yan, B. Xu, J. Z. Sun, W. Tian, Z. Zhao, A. Qin, B. Z. Tang, *Chem. Sci.* **2015**, *6*, 1932.

[9] a) M. Chen, H. Nie, B. Song, L. Li, J. Z. Sun, A. Qin, B. Z. Tang, *J. Mater. Chem. C* **2016**, *4*, 2901; b) Y. Jiang, L. Sun, J. Du, Y. Liu, H. Shi, Z. Liang, J. Li, *Cryst. Growth Des.* **2017**, *17*, 2090; c) L. Pan, W. Luo, M. Chen, J. Liu, L. Xu, R. Hu, Z. Zhao, A. Qin, B. Z. Tang, *Chin. J. Org. Chem.* **2016**, *36*, 1316.

[10] a) R. J. Reiffenstein, W. C. Hulbert, S. H. Roth, *Annu. Rev. Pharmacol. Toxicol.* **1992**, *32*, 109; b) R. O. Beauchamp, J. S. Bus, J. A. Popp, C. J. Boreiko, D. A. Andjelkovich, P. Leber, *CRC Crit. Rev. Toxicol.* **2008**, *38*, 25.

[11] a) K. Abe, H. Kimura, *J. Neurosci.* **1996**, *16*, 1066; b) J. C. Savage, D. H. Gould, *J. Chromatogr., Biomed. Appl.* **1990**, *526*, 540.

**ADVANCED
SCIENCE NEWS**

www.advancedsciencenews.com

**ADVANCED
FUNCTIONAL
MATERIALS**

www.afm-journal.de

[12] a) K. Eto, T. Asada, K. Arima, T. Makifuchi, H. Kimura, *Biochem. Biophys. Res. Commun.* **2002**, *293*, 1485; b) M. Whiteman, J. S. Armstrong, S. H. Chu, S. J. Ling, B. S. Wong, N. S. Cheung, B. Halliwell, P. K. Moore, *J. Neurochem.* **2004**, *90*, 765; c) M. Yusuf, B. T. K. Huat, M. Whiteman, M. Bhatia, P. K. Moore, *Biochem. Biophys. Res. Commun.* **2005**, *333*, 1146; d) S. K. Jain, R. Bull, J. L. Rains, P. F. Bass, S. N. Levine, S. Reddy, R. McVie, J. A. Bocchini Jr., *Antioxid. Redox Signal.* **2010**, *12*, 1333.

[13] a) V. S. Lin, W. Chen, M. Xian, C. J. Chang, *Chem. Soc. Rev.* **2015**, *44*, 4596; b) L. A. Montoya, T. F. Pearce, R. J. Hansen, L. N. Zakharov, M. D. Pluth, *J. Org. Chem.* **2013**, *78*, 6550; c) B. W. Miche, A. R. Lippert, C. J. Chang, *J. Am. Chem. Soc.* **2012**, *134*, 15668; d) S. Yang, Y. Qi, C. Liu, Y. Wang, Y. Zhao, L. Wang, J. Li, W. Tan, R. Yang, *Anal. Chem.* **2014**, *86*, 7508; e) C. Liu, J. Pan, S. Li, Y. Zhao, L. Y. Wu, C. E. Berkman, A. R. Whorton, M. Xian, *Angew. Chem., Int. Ed.* **2011**, *50*, 10327; f) X. Yang, Y. Ren, Z. Gao, *Chem. Eur. J.* **2015**, *21*, 988.

[14] a) H. Peng, Y. Cheng, C. Dai, A. L. King, B. L. Predmore, D. J. Lefer, B. Wang, *Angew. Chem., Int. Ed.* **2011**, *50*, 9672; b) K. Sasakura, K. Hanaoka, N. Shibuya, Y. Mikami, Y. Kimura, T. Komatsu, T. Ueno, T. Takuya, H. Kimura, T. Nagano, *J. Am. Chem. Soc.* **2011**, *133*, 18003; c) Y. Chen, C. Zhu, Z. Yang, J. Chen, Y. He, Y. Jiao, W. He, L. Qiu, J. Cen, Z. Guo, *Angew. Chem., Int. Ed.* **2013**, *52*, 1688.

[15] Y. Cai, L. Li, Z. Wang, J. Z. Sun, A. Qin, B. Z. Tang, *Chem. Commun.* **2014**, *50*, 8892.

[16] a) X. Zhang, Z. Chi, Y. Zhang, S. Liu, J. Xu, *J. Mater. Chem. C* **2013**, *1*, 3376; b) G. Zhang, J. Lu, M. Sabat, C. L. Fraser, *J. Am. Chem. Soc.* **2010**, *132*, 2160; c) Y. Sagara, T. Komatsu, T. Ueno, K. Hanaoka, T. Kato, T. Nagano, *Adv. Funct. Mater.* **2013**, *23*, 5277; d) N. Mizoshita, T. Tani, S. Inagaki, *Adv. Mater.* **2012**, *24*, 3350.

[17] a) Z. Chi, X. Zhang, B. Xu, X. Zhou, C. Ma, Y. Zhang, S. Liu, J. Xu, *Chem. Soc. Rev.* **2012**, *41*, 3878; b) Y. Q. Dong, J. W. Y. Lam, B. Z. Tang, *J. Phys. Chem. Lett.* **2015**, *6*, 3429.

[18] a) J. Tong, Y. Wang, J. Mei, J. Wang, A. Qin, J. Z. Sun, B. Z. Tang, *Chem. Eur. J.* **2014**, *20*, 4661; b) Z. F. Chang, L. M. Jing, C. Wei, Y. P. Dong, Y. C. Ye, Y. S. Zhao, J. L. Wang, *Chem. Eur. J.* **2015**, *21*, 8504; c) C. Niu, Y. You, L. Zhao, D. He, N. Na, J. Ouyang, *Chem. Eur. J.* **2015**, *21*, 13983; d) N. Zhao, M. Li, Y. Yan, J. W. Y. Lam, Y. L. Zhang, Y. S. Zhao, K. S. Wong, B. Z. Tang, *J. Mater. Chem. C* **2013**, *1*, 4604; e) Q. Qi, J. Qian, X. Tan, J. Zhang, L. Wang, B. Xu, B. Zou, W. Tian, *Adv. Funct. Mater.* **2015**, *25*, 4005; f) H. T. Feng, J. B. Xiong, J. Luo, W. F. Feng, D. Yang, Y. S. Zheng, *Chem. Eur. J.* **2017**, *23*, 644.

[19] a) X. Luo, J. Li, C. Li, L. Heng, Y. Q. Dong, Z. Liu, Z. Bo, B. Z. Tang, *Adv. Mater.* **2011**, *23*, 3261; b) Y. Dong, J. W. Y. Lam, A. Qin, J. Sun, J. Liu, Z. Li, J. Sun, H. H. Y. Sung, I. D. Williams, H. S. Kwok, B. Z. Tang, *Chem. Commun.* **2007**, 3255.

[20] T. Han, Y. Dong, N. Xie, S. Chen, N. Zhao, E. Zhao, J. W. Y. Lam, H. H. Y. Sung, Y. Dong, B. Tong, B. Z. Tang, *J. Mater. Chem. C* **2013**, *1*, 7314.

[21] a) M. S. Kwon, J. Gierschner, S. J. Yoon, S. Y. Park, *Adv. Mater.* **2012**, *24*, 5487; b) H. J. Kim, D. R. Whang, J Gierschner, C. H. Lee, S. Y. Park, *Angew. Chem., Int. Ed.* **2015**, *54*, 4330.

[22] a) M. Chen, L. Li, H. Nie, Y. Shi, J. Mei, J. Wang, J. Z. Sun, A. Qin, B. Z. Tang, *Chem. Commun.* **2015**, *51*, 10710; b) L. Li, H. Nie, M. Chen, J. Sun, A. Qin, B. Z. Tang, *Faraday Discuss.* **2017**, *196*, 245; c) Z. F. An, C. Zheng, R. F. Chen, J. Yin, J. J. Xiao, H. F. Shi, Y. Tao, Y. Qian, W. Huang, *Chem. Eur. J.* **2012**, *18*, 15655; d) W. Qin, K. Li, G. Feng, M. Li, Z. Yang, B. Liu, B. Z. Tang, *Adv. Funct. Mater.* **2014**, *24*, 635; e) W. Qin, D. Ding, J. Liu, W. Z. Yuan, Y. Hu, B. Liu, B. Z. Tang, *Adv. Funct. Mater.* **2012**, *22*, 771.

[23] a) Y. Hong, J. W. Y. Lam, B. Z. Tang, *Chem. Commun.* **2009**, 4332; b) Y. Hong, J. W. Y. Lam, B. Z. Tang, *Chem. Soc. Rev.* **2011**, *40*, 5361.

[24] Q. Wu, T. Zhang, Q. Peng, D. Wang, Z. Shuai, *Phys. Chem. Chem. Phys.* **2014**, *16*, 5545.

[25] H. Li, X. Feng, Y. Guo, D. Chen, R. Li, X. Ren, X. Ren, X. Jiang, Y. Dong, B. Wang, *Sci. Rep.* **2014**, *4*, 4366.

[26] J. Mei, J. Z. Sun, B. Z. Tang, *Dyes Pigm.* **2017**, *141*, 366.

[27] X. Luo, Y. Hong, S. Chen, C. W. T. Leung, N. Zhao, B. Situ, J. W. Y. Lam, B. Z. Tang, *Sci. Rep.* **2014**, *4*, 4272.

[28] a) X. Li, F. Huo, Y. Yue, Y. Zhang, C. Yin, *Sens. Actuators, B* **2017**, *253*, 42; b) K. Liu, Y. Hu, Z. Xu, M. Yin, *Anal. Chem.* **2017**, *89*, 5131; c) M. Y. Wu, T. He, K. Li, M. B. Wu, Z. Huang, X. Q. Yu, *Analyst* **2013**, *138*, 3018.

[29] a) T. Chatterjee, B. C. Ranu, *RSC Adv.* **2013**, *3*, 10680; b) M. Oba, K. Tanaka, K. Nishiyama, W. Ando, *J. Org. Chem.* **2011**, *76*, 4137; c) D. D. Monte, G. Bellomo, H. Thor, P. Nicotera, S. Orrenius, *Arch. Biochem. Biophys.* **1984**, *235*, 343; d) P. Eaton, *Free Radical Biol. Med.* **2006**, *40*, 1889; e) J. Ying, N. Clavreul, M. Sethuraman, T. Adachi, R. A. Cohen, *Free Radical Biol. Med.* **2007**, *43*, 1099.

[30] a) F. C. Spano, *Acc. Chem. Res.* **2010**, *43*, 429; b) Y. Egawa, R. Hayashida, J. I. Anzai, *Langmuir* **2007**, *23*, 13146; c) N. Maiti, S. Mazumdar, N. Periasamy, *J. Phys. Chem. B* **1998**, *102*, 1528; d) O. J. Dautel, G. Wantz, R. Almaiac, D. Flot, L. Hirsch, J. P. Lere-Porte, J. P. Parneix, F. Serein-Spirau, L. Vignau, J. J. E. Moreau, *J. Am. Chem. Soc.* **2006**, *128*, 4892; e) T. Hasobe, S. Fukuzumi, P. V. Kamat, *J. Am. Chem. Soc.* **2005**, *127*, 11884.